Cellular and Molecular Biology

C M B Association Publisher

Journal homepage: www.cellmolbiol.org

PLGA-Au-PFH-NPs-based Ultrasound Imaging in Detecting Fetal Spinal Deformities

Xiuxiu Hao[1], Zhigang Cheng[2], Longxia Wang[3], Yihua He[4], Cuijing Chen[1], Ping Liang[2*]

[1]*Department of Ultrasound, Fifth Medical Center, PLA General Hospital, Beijing 100071, China*
[2]*Department of Interventional Ultrasound, First Medical Center of PLA General Hospital, Beijing 100853, China*
[3]*Department of Ultrasound Diagnosis, First Medical Center of PLA General Hospital, Beijing 100853, China*
[4]*The Maternal Fetal Medical Consultation Center, Beijing Anzhen Hospital, Capital Medical University, Beijing 100029, China*

ARTICLE INFO

Original paper

Article history:
Received: September 01, 2021
Accepted: March 02, 2022
Published: March 31, 2022

Keywords:
fetus; spinal abnormalities; ultrasound imaging; PLGA; carbon nano materials; liquid fluorocarbon

ABSTRACT

The study focused on the performance of ultrasound imaging in detecting fetal spinal deformities. First, the double emulsification method and the carbodiimide method were used to prepare the target Au-loaded nanorod phase-change nano-level contrast agent-PLGA-Au-PFH-NPs. After being characterized for physical and chemical properties, it was used in ultrasound imaging diagnosis. The results showed that the prepared PLGA-Au-PFH-NPs solution was a milky white suspension, the particle size detected by the laser particle sizer was (376.17±20.74) nm, and the Zeta potential was (-4.82±2.88) mV. Under the light microscope, it showed a spherical shape, uniform size distribution, and a very smooth surface. The encapsulation rate measured by the UV spectrophotometer was (80.63±4.82) %, and there was no significant difference in cell survival rate between different concentrations ($P>0.05$). Prenatal ultrasound in the observation group accurately diagnosed 10 cases with spinal deformities, and the diagnostic accuracy rate was 50%, including 5 cases of meningocele, 3 cases of invisible spina bifida, 1 case of myelomeningocele, and 1 case of hemivertebrae. In the control group, 7 cases were diagnosed correctly by conventional ultrasound, and the diagnosis accuracy rate was 35%, including 3 cases of meningocele, 3 cases of invisible spina bifida, and 1 case of hemivertebra. The diagnostic accuracy of the observation group was higher than that of the control group, and the difference was statistically significant ($P<0.05$). In conclusion, the prepared PLGA-Au-PFH-NPs had good physical and chemical properties. Ultrasound imaging based on the PLGA-Au-PFH-NPs had high accuracy in diagnosing fetal spinal deformities. To a certain extent, it provides a basis for clinical diagnosis of fetal spinal abnormality and some new ideas for ultrasound imaging diagnosis.

DOI: http://dx.doi.org/10.14715/cmb/2022.68.3.3

Introduction

Abnormal spine development is a common fetal malformation (1). The abnormal development of the fetal spine and spinal cord are interrelated and affect each other. Abnormal development of the spine may be accompanied by spinal cord diseases, and abnormal development of the spinal cord can cause changes in the morphology of the spine. As imaging technology is gradually being mature, ultrasound has become popular in the diagnosis of fetal malformations (2). However, the tissue resolution and spatial resolution of ultrasound imaging are low, and the imaging quality is severely affected by many factors, so certain anatomical structures, such as the fetal spinal cord, and pathological changes cannot be ideally described (3). Two-dimensional ultrasound has a high misdiagnosis rate for fetal limb and spinal dysplasia, especially limbs, hands, and feet dysplasia (4). Three-dimensional surface mode, transparent mode, and plane mode can reconstruct three-dimensional images of the fetal body surface and bones, which provides a basis for the accurate diagnosis of fetal spine and limb abnormalities (5,6).

With the development of imaging technology, molecular imaging technology has become a research hotspot. Photoacoustic imaging is a new non-invasive biomedical imaging method (7). The photoacoustic signal generated by biological tissue absorbs the light so that it can obtain molecular-level image information, and perform multi-scale high-resolution imaging of the tissue (8). Among nanomaterials, gold nanorods (GNRs) have been highly valued due to their unique

---

*Corresponding author. E-mail: zhuniann1980@163.com

optical, optoelectronic, photothermal, photochemical, and molecular biological properties (9). GNRs are easy to synthesize, have good stability and low toxicity, and are suitable for the preparation of molecular probes (10). GNRs can detect pathological features at the molecular level because they have unique tunable surface plasmon resonance (SPR) optical properties and a high light-absorption coefficient. Research has pointed out that the absorption and scattering intensity of Au nanoparticles is higher than that of most organic dye molecules, which makes them have obvious advantages in imaging.

Multifunctional liquid fluorocarbon emulsion is a nano-level contrast agent that can be used for multi-modality imaging (ultrasound, photoacoustics, MRI, and CT). Liquid perfluorocarbons can irradiate light through photo-induced phase change (ODV), which can be widely used in biomedical testing. Using the ODV method, the liquid fluorocarbon emulsion can evaporate from droplets to microbubbles (ie phase change), thereby increasing the acoustic impedance of surrounding tissue and improving the quality of ultrasound imaging. Polylactic acid oxalic acid (PLGA) is a biodegradable polymer approved by the FDA, using lactic acid and oxalic acid as degrading agents. Because of the low toxicity, it has a good film-forming ability. PLGA and its products are extensively used in nano-medicine.

Above, in this study, a highly-active nano-molecular probe was prepared, which was loaded with liquid fluorocarbon-perfluorohexane (PFH) and GNRs. The optical properties of GNRs can enhance the photoacoustic imaging, and the phase change properties of liquid fluorocarbon can increase the acoustic impedance around the tissue, thereby highlighting the tissue boundary of the region of interest (RoI) to enhance the ultrasound imaging. This study aimed to provide new ideas for the diagnosis of fetal malformations, thereby improving the accuracy of diagnosis and preventing fetal malformations.

Materials and methods

Research subjects

In this study, 20 pregnant women with suspected fetal malformations, admitted to the hospital from March 20, 2019 to March 20, 2020, were selected as the research subjects, and they were randomly divided into control group and observation group, each with 10 patients. The control group was diagnosed by conventional ultrasound, and the observation group was diagnosed by ultrasound imaging based on PLGA liquid fluorocarbon nanoparticles. The study has been approved by the Medical Ethics Committee of the Hospital, and the patients and their families understood the situation and signed an informed consent form.

Main instruments and reagents

GE-E8/730, PHILIPS-iu22 ultrasonic diagnostic equipment, abdominal convex array probe, and three-dimensional volume probe were purchased from Jiangsu Medical Instruments Co., Ltd., with a frequency of 3~5MHz and power of less than 100mW/cm^2.

Main reagents: PLGA-COOH, Au-NRs (GNR) (NR-10-780), DAPI, CCK-8, etc. were purchased from Jiangsu Medical Reagent Co., Ltd., phosphate buffer solution (PBS, pH 7.4), perfluorinated Hexane (PFH), polyvinyl alcohol (PVA), physiological saline, etc. were purchased from Shanghai Biyuntian Biotechnology Co., Ltd.

Phase-change nanoparticles loaded with GNRs

[1] The nanoprobe was prepared by the double emulsification method, and 200μL of PFH was added to 100uL of GNR solution. Under an ice environment, the white primary emulsion was acquired by acoustic vibration for 1 min (operating cycle 5:5.103 w);

[2] 5mL of dichloromethane was added to 50 mg of PLGA-COOH, followed by ultrasonic cleaning. After fully dissolved, the above-mentioned primary emulsion was added to the PLGA dichloromethane solution, followed by acoustic vibration for 5 minutes to obtain a white complex emulsion;

[3] 5mL of 5% polyvinyl alcohol (PVA) was added to the double emulsion, followed by homogenization for 5 minutes;

[4] 15mL 2% isopropanol was added to solidify the surface of the nanoparticles;

[5] the liquid was stirred with a magnetic stirrer for 2 hours to completely volatilize the dichloromethane;

[6] centrifugation was performed twice using a high-speed low-temperature centrifuge (10000 r/min, 10 min), and the centrifuge was cleaned with double distilled water, and GNR-PFH-PLGA nanoparticles were collected;

[7] the carbodiimide method was used to modify the nanoprobe, and the non-targeted nanoparticles were dissolved in 3 mL of MES buffer (0.1 mol/L, pH 5.5);

[8] coupling activators of EDC and NHS were added, followed by an ice bath for 1h (EDC:NHS molar ratio=1:3, PLGA:EDC molar ratio=1:10);

[9] after centrifugation and washing with PBS 3 times, the nanoparticles were re-dissolved in MES buffer (0.1 mol/L, pH 8);

[10] after centrifugation and washing with PBS 3 times, targeted nanoparticles were obtained (PLGA-Au-PFH-NPs).

Au-NPs of different diameters and the Au foil are shown in Figure 1.

Figure 1. The colors of Au-NPs of different diameters (left) and the Au foil (right)

Characterization of PLGA-Au-PFH-NPs nanoparticles

The size and uniformity were visualized with an optical microscope (11). Malvern laser particle size detection instrument and Zeta potential detector were used to detect particle size and surface potential. Its surface morphology and internal structure were observed with a transmission electron microscope and scanning electron microscope. An ultraviolet spectrophotometer was used to calculate the encapsulation efficiency of GNRs in NPs. 1 mL of NPs was centrifuged to separate the supernatant at low temperature, and the absorbance of the supernatant was measured at a wavelength of 780 nm. The content of GNRs in the supernatant was calculated using the standard equation, and then the encapsulation rate was calculated as follows: A represents the total input of GNRs, B represents the input of GNRs, and C represents the amount of GNRs in the supernatant. Figure 2 shows the zeta potential detector.

$$Encapsulation\ rate = \frac{B-C}{A} \tag{1}$$

Figure 2. Zeta potential detector

Phase-change ability detection

The prepared NPs were irradiated with an 808nm laser treatment instrument for 10 minutes. Before and after the laser irradiation, the shape and size of each group of NPs were observed with an optical microscope and the temperature before and after irradiation was recorded with an infrared thermal imager.

The effect of PLGA-Au-PFH-NPs on cell viability

CCK-8 was used to detect the cytotoxicity of the nanoparticles (12); and cells were cultured in vitro and seeded in a 96-well plate during the logarithmic growth phase, followed by culture for 24 hours. The NPs solution was diluted into five different concentrations with 1640 medium: 2mg/mL, 3mg/mL, 5mg/mL, 10mg/mL, 20mg/mL. Each group was transferred to culture wells, and 5 replicate wells were set for each concentration, followed by incubation for 24 hours. The cell morphology was observed by a light microscope, and the cell activity was detected by the CCK8 method.

Two-dimensional ultrasound diagnosis

Two-dimensional ultrasound (13): the pregnant woman lay on her back and, if necessary, lay on her side on the bed. First of all, the biological indicators of pregnant women were measured and the fetus was screened at level III. The examination focused on the development of the spine and limbs. Spine examination included the shape and arrangement of the entire spine and each segment, as well as the integrity of the vertebral body and vertebral arch. The upper and lower limbs were scanned carefully to collect clear images. Upper extremity scanning included the long axis of the humerus and its length, the contours of the forearm, the longitudinal section of the forearm ulna and radius, and the presence or absence of the ulna and radius. Additionally, the wrist, palm, fingers, and metacarpal bones were scanned, and the hand shape and its positional relationship with the forearm were observed. Lower extremity scanning included the long axis of the femur and its length, the long axis of the tibia and fibula of the lower leg, as well as the ankle, palm and toe. The shape of the foot and its positional relationship with the calf were then observed.

Three-dimensional ultrasound diagnosis

Three-dimensional ultrasound refers to three-dimensional imaging and real-time three-dimensional dynamic observation of all spine and limbs. Under the 3D mode, the volume probe was used, and 3D reconstruction was then performed. The RoI was observed from multiple angles. The morphological structure and development of the fetal limbs and the integrity of the spine skin surface were displayed by surface imaging. The development of the fetal spine and limb bones was presented by transparent imaging. The arrangement and various vertebral bodies, the integrity of the vertebral body, and the development and existence of limb bones were observed. The overall shape and development of each vertebral body and vertebral arch were visualized from multiple angles of the spatial rotating image. Under the four-dimensional mode, dynamic three-dimensional images were obtained in real-time under the surface mode. The structural shape and activity state of the limbs and spine were dynamically observed, and the x, y and z axes were adjusted to obtain the best results (14).

Statistical methods

The data was processed by SPSS19.0 version statistical software, the measurement data were expressed by the mean ± standard deviation ($\bar{x}\pm s$), and the count data were expressed by a percentage (%). $P<0.05$ was the threshold for significance.

Results and discussion

Characterization results of PLGA-Au-PFH-NPs

The PLGA-Au-PFH-NPs solution prepared in this study was a milky white suspension. The particle size detected by the laser particle sizer was (376.17±20.74) nm, and the Zeta potential was (-4.82±2.88) mV. Under the light microscope, the NPs were sphere-like in shape, the size distribution was uniform, and the surface was very smooth. Under the scanning electron microscope, it was noted that the nanoparticles were spherical and arranged regularly (Figures 3, 4 and 5). Gold nanorods were attached to the surface of the NPs. The encapsulation rate measured by the ultraviolet spectrophotometer was (80.63±4.82) %. The NPs were scanned at full wavelength, and the maximum absorption peak was measured near 800nm.

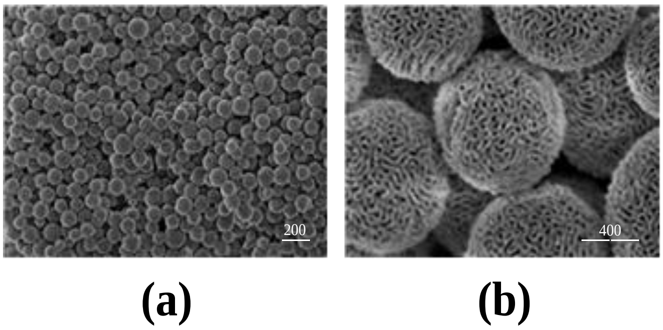

(a) (b)

Figure 3. Microscopic observation results of PLGA-Au-PFH-NPs of different sizes, (a) × 200 image, (b) × 400 image

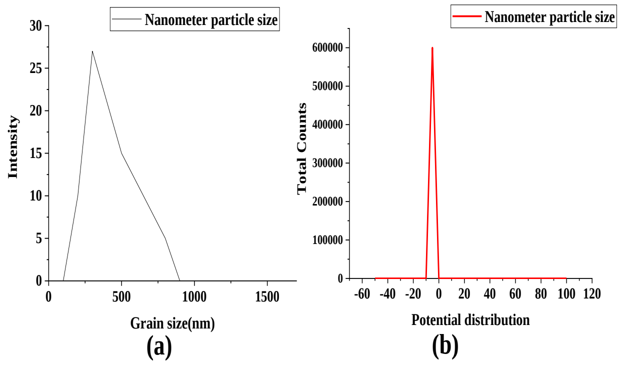

(a) (b)

Figure 4. Size of PLGA-Au-PFH-NPs(a); potential distribution of PLGA-Au-PFH-NPs (b)

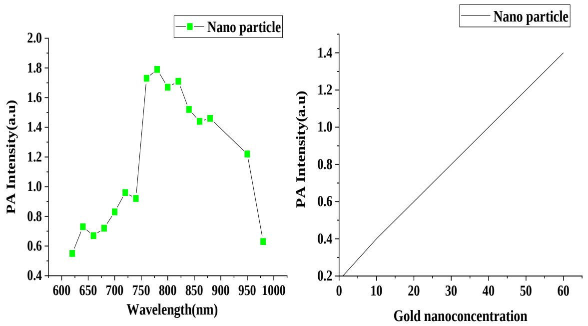

(a) (b)

Figure 5. The PA value of PLGA-Au-PFH-NPs scanned at the full wavelength (a); the absorbance concentration correlation curve of Au-NPs in the UV-Vis-NIR region with a wavelength of 780 nm (b)

The effect of PLGA-Au-PFH-NPs on cell activity

The CCK-8 experiment confirmed that different concentrations of NPs had no effect on cell viability (Figure 6), and the cell survival rate under different concentrations all exceeded 80%. There was no significant difference in cell survival rate between different concentrations ($P>0.05$).

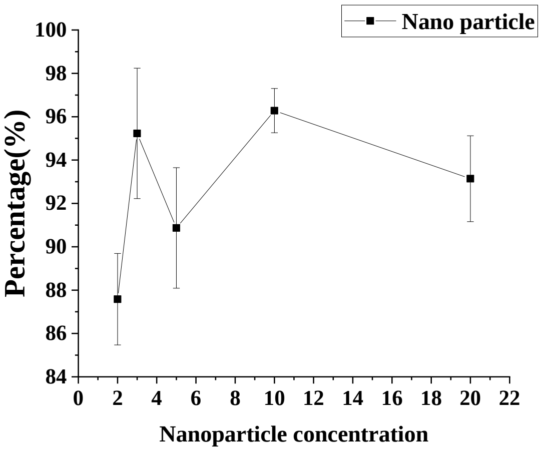

Figure 6. The effect of PLGA-Au-PFH-NPs on cell viability

Phase-change ability detection of PLGA-Au-PFH-NPs

PLGA-Au-PFH-NPs were circular and uniform in size when observed under a light microscope (Figure 7). After laser irradiation, the PFHliquid wrapped in the PLGA-Au-PFH-NPs vaporized and became gas. The diameter of the NPs began to increase, and some nanoparticles even burst under radiation.

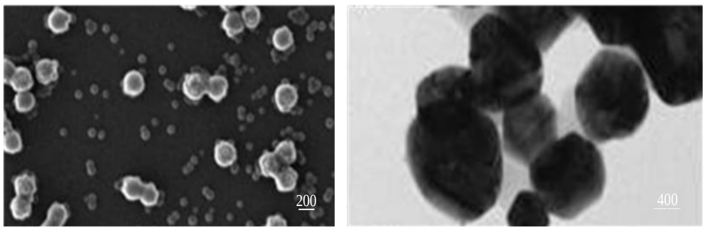

(a) (b)

Figure 7. PLGA-Au-PFH-NPs before and after irradiation. (a) before radiation; (b) after radiation

General information of the two groups of patients

The age of 20 pregnant women included in this study ranged from 20 to 38 years old. In the control group, the average age was (24.18±3.39) years, the average weight was (60.82±4.02), and the average gestational age was (28.18±4.71) weeks. In the observation group, the average age was (25.01±4.02) years, the average weight was (62.19±3.22), and the average gestational age was (29.84±3.19) weeks (Figure 8). There was no statistical difference between the two groups and they were comparable ($P>0.05$).

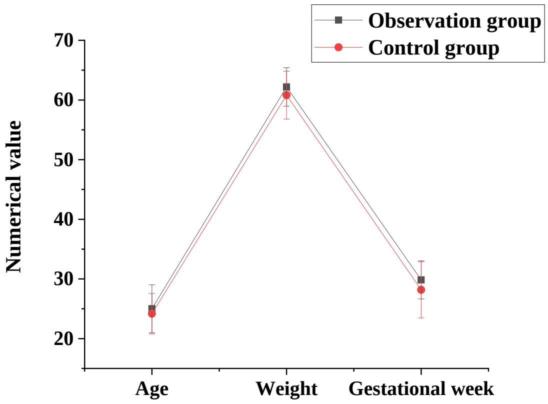

Figure 8. General information of the two groups of patients.

Ultrasound examination results of the two groups of patients

A total of 20 fetuses were detected in 20 pregnant women, including 11 cases of irregular spinal arrangement, 5 cases of limited spinal canal widening, and 4 cases of abnormal spinal flexion. Among the 11 fetuses with irregular spine arrangement, 5 had meningocele, 3 had invisible spina bifida, 1 had myelomeningocele, 1 had hemivertebrae, and 1 had butterfly vertebra with longitudinal myelopathy (Figure 9). Some ultrasound images of the observation group were as follows (Figure 10).

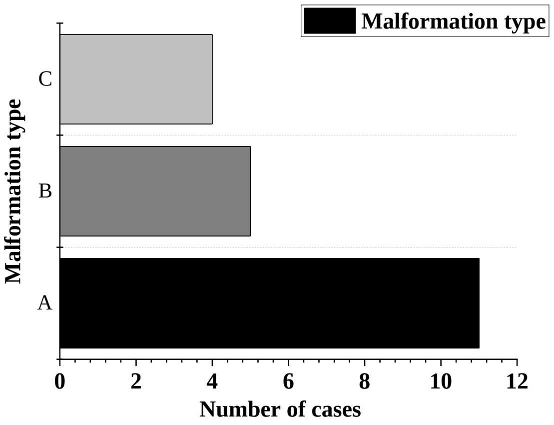

Figure 9. Types of fetal spinal deformity. A: the irregular arrangement of the spine; B: the limited widening of the spinal canal; C: the invisible spina bifida

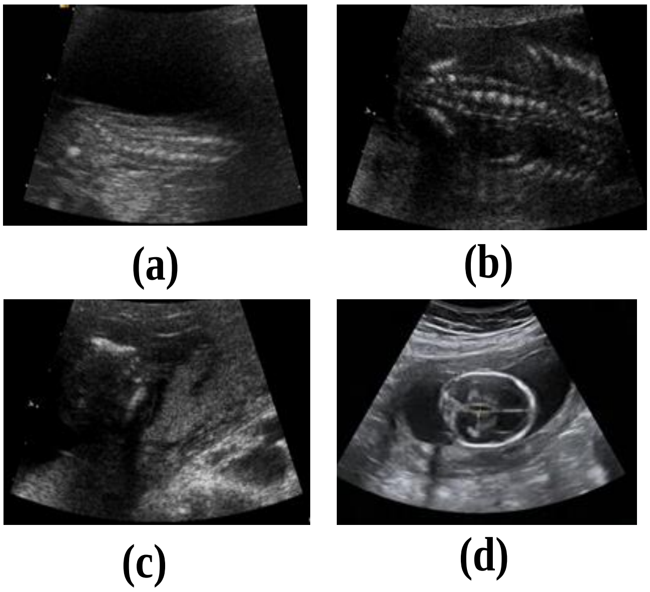

Figure 10. Ultrasound images of fetal spina bifida. (a) Sagittal section; (b) Coronal section; (c) Cross-section; (d) 27 weeks of gestation, fetal spina bifida and hydrocephalus

Ultrasound diagnosis results

As for the ultrasound diagnosis results of the two groups of patients, the observation group accurately diagnosed 10 fetuses with spinal abnormalities by prenatal ultrasound, and the accuracy rate was 50%, including 5 cases of meningocele, 3 cases of invisible spina bifida, 1 case of myelomeningocele, and 1 case of hemivertebrae. In the control group, 7 cases were correctly diagnosed by conventional ultrasound, and the diagnostic accuracy rate was 35%, including 3 cases of meningocele, 3 cases of invisible spina bifida, and 1 case of hemivertebra (Figure 11). The diagnostic accuracy of the observation group was higher than that of the control group, and the difference was statistically significant ($P<0.05$).

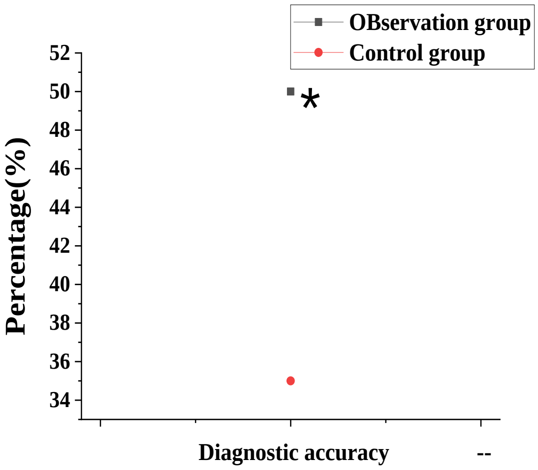

Figure 11. Comparison of the diagnostic accuracy of the two groups of patients. * indicated that the observation group and the control group were statistically different ($P<0.05$)

Ultrasonography is a common imaging method for the fetal spine and limbs. CT and X-ray examinations affect the development of the fetus to a certain extent. Currently, prenatal ultrasound screening is mainly based on two-dimensional diagnosis, which can screen out the abnormal development of most fetal organs (15). Abnormal development of the spine and limbs is a common deformity. Spina bifida is a serious neural tube deformity. Osteogenesis, atrophy, and loss of limbs are all serious deformities (16). Therefore, the prenatal diagnosis of abnormal fetal spine and limb development is very important. To improve the accuracy of prenatal diagnosis, first, the double emulsification method and carbodiimide method were used to prepare PLGA-Au-PFH-NPs. NPs have great potential in PA imaging.

The prepared PLGA-Au-PFH-NPs solution was a milky white suspension. The particle size detected by the laser particle sizer was (376.17±20.74) nm, and the Zeta potential was (-4.82±2.88) mV. Under the light microscope, it was spherical in shape with uniform size distribution, and the surface was very smooth. Under the scanning electron microscope, the nano-particles were spherical and arranged neatly and regularly. GNRs were attached to the surface of the NPs, and the encapsulation rate measured by the UV spectrophotometer was (80.63±4.82) %. The NPs were scanned at full wavelength, and the maximum absorption peak was measured near 800nm; CCK-8 experiments confirmed that different concentrations of NPs had no effect on cell viability, and the cell survival rate of each group of concentrations exceeded 80%. There was no significant difference in cell survival rate between different concentrations ($P>0.05$); PLGA-Au-PFH-NPs were circular and uniform in size when observed under a light microscope. After laser irradiation, the PFH wrapped in the PLGA-Au-PFH-NPs group underwent a liquid-vapor phase transition, and the diameter of the NPs began to increase, and some nanoparticles even burst under continuous radiation. This was in line with the research conclusion of Koerner et al. (2019) (17), which indicated that the nanoparticle had a small particle size and can circulate in blood vessels. Under a full wavelength scan, the maximum absorption peak appeared near 800nm, which proved that the GNRs loaded with PFH did not affect the optical properties and can perform dual-mode ultrasound imaging. The temperature of the PLGA-Au-PFH-NPs began to change after being irradiated by the laser, which indicated that the nanoparticles can remain stable at room temperature, and the PFH phase transition temperature was 56°C. Cell viability studies have shown that the concentration of NPs had no effect on cell viability, and cell survival rates under different concentrations of NPs were all above 80%. This indicated that PLGA-Au-PFH-NPs were safe.

Organic and inorganic nanoparticles with unique properties compared to bulk materials may be a desirable carrier for the therapy and diagnosis of various diseases (18-20). The prepared PLGA-Au-PFH-NPs contrast agent was applied to the ultrasound diagnosis of pregnant women. Of the 20 fetuses with spinal deformities, there were 11 cases of irregular spinal arrangement, 5 cases of limited spinal canal widening, and 4 cases of abnormal spinal flexion. Of the 11 fetuses with irregular spine arrangement, 5 had meningocele, 3 had invisible spina bifida, 1 had myelomeningocele, 1 had hemivertebrae, and 1 had butterfly vertebra with longitudinal myelopathy. The observation group accurately diagnosed 10 fetuses with spinal deformities by prenatal ultrasound, and the accuracy rate was 50%, including 5 cases of meningocele, 3 cases of invisible spina bifida, 1 case of myelomeningocele, and 1 case of hemivertebrae. In the control group, 7 cases were correctly diagnosed by conventional ultrasound, and the diagnostic accuracy rate was 35%, including 3 cases of meningocele, 3 cases of invisible spina bifida, and 1 case of hemivertebra. The diagnostic accuracy of the observation group was higher than that of the control group, and the difference was statistically significant ($P<0.05$). Song et al. (2019) (21) have shown that ultrasound can clearly detect and diagnose spina bifida, spina bifida, obvious occult spina bifida, and spina bifida. However, ultrasound imaging of arachnoid cysts in the spinal canal, tethered spinal cord, and syringomyelia show that the spinal column is arranged irregularly or the spinal cord dilatation is limited, but the spinal cord cannot be observed. As a result, it is impossible to identify whether myelomeningocele, meningocele, and meningocele are combined with myelodysplasia, so the accuracy of ultrasound imaging diagnosis is generally low. The research of Sahu et al. (2020) (22) pointed out that three-dimensional ultrasound and maximum mode imaging can clearly and comprehensively display the anatomical shape and connection relationship of the spine and ribs, and diagnose deformities, such as hemivertebrae and rib misalignment. This was also confirmed in the study of Toledo et al. (2019) (23).

Conclusion

In the study, the double emulsification method and the carbodiimide method were used to prepare PLGA-Au-PFH-NPs. After being characterized for its physical and chemical properties, it was applied to the ultrasound imaging diagnosis of fetal spinal deformities. The results showed that the prepared PLGA-Au-PFH-NPs had good physical and chemical properties, and the ultrasound imaging based on PLGA-Au-PFH-NPs had high accuracy in diagnosing fetal spinal abnormalities. However, there are still some shortcomings in this study. Their lack of a control experiment of NPs prepared. Therefore, the experimental results are subjective. Furthermore, the sample size is small, which reduces the power of the study. In the follow-up, expanded sample size is needed to strengthen the findings of the study. In conclusion, the PLGA-Au-PFH-NPs contrast agent can lift the diagnosis accuracy of spinal deformities. To a certain extent, this study provides a basis for clinical diagnosis of fetal spinal abnormality and some new ideas for ultrasound imaging diagnosis.

Acknowledgments

None

Conflict interest

The authors declare no conflict of interest.

References

1. Yang K, Zhu J, Tan Y, Sun X, Zhao H, Tang G, Zhang D, Qi H. Whole-exome sequencing identified compound heterozygous variants in ROR2 gene in a fetus with Robinow syndrome. J Clin Lab Anal 2020; 34(2): e23074.

2. Gao JX, Zhu JA, Pei QY, Li JG. Prenatal ultrasonic diagnosis and differential diagnosis of isolated right aortic arch with mirror-image branching. Arch Gynecol Obstet 2017; 295(5): 1291-1295.

3. Miskin M, Baim RS, Allen LC, Benzie RJ. Ultrasonic assessment of the fetal spine before 20 weeks' gestation. Radiology 1979; 132(1): 131-5.

4. Robinson AJ, Russell S, Rimmer S. The value of ultrasonic examination of the lumbar spine in infants with specific reference to cutaneous markers of occult spinal dysraphism. Clin Radiol 2005; 60(1): 72-7.

5. Xiong Z, Zeng S, Chen HX, Qiu X, Tang G. Unique finding in congenital muscular torticollis: Clinic screening on the neck of one day old neonate and ultrasonographic imaging from birth through 3 years of follow-up. Medicine (Baltimore) 2019; 98(11): e14794.

6. Kulovaný E, Safár P. Prenatální ultrazvuková diagnostika vrozených vývojových vad. I. Uvod, patologie hlavy, pátere a hrudníku [Prenatal ultrasonic diagnosis of congenital developmental defects. I. Introduction, pathology of the head, spine and thorax]. Cesk Gynekol 2015; 55(2): 134-41.

7. Kim TK, Noh SY, Wilson SR, Kono Y, Piscaglia F, Jang HJ, Lyshchik A, Dietrich CF, Willmann JK. Contrast-enhanced ultrasound (CEUS) liver imaging reporting and data system (LI-RADS) 2017 - a review of important differences compared to the CT/MRI system. Clin Mol Hepatol 2017; 23(4): 280-289.

8. Dias T, Sairam S, Kumarasiri S. Ultrasound diagnosis of fetal renal abnormalities. Best Pract Res Clin Obstet Gynaecol 2014; 28(3): 403-15.

9. Cong X, Sun X, Liu S. Evaluation and screening ultrasonic signs in the diagnosis of fetal biliary cystic malformation. J Matern Fetal Neonatal Med 2015; 28(17): 2100-5.

10. Li XS, Xia HM, Wang D, Zhu JK, Ran JH. The Ultrasonic Microsurgical Anatomical Comparative Study of the CHD Fetuses and Their Clinical Significance. Biomed Res Int 2015; 2015: 520394.

11. Lu JW, Lin L, Xiao LP, Li P, Shen Y, Zhang XL, Zhang M, Yu MX, Zhang YZ. Prognosis of 591 fetuses with ultrasonic soft markers during mid-term pregnancy. J Huazhong Univ Sci Technolog Med Sci 2017; 37(6): 948-955.

12. Sabbagha RE, Sheikh Z, Tamura RK, DalCompo S, Simpson JL, Depp R, Gerbie AB. Predictive value, sensitivity, and specificity of ultrasonic targeted imaging for fetal anomalies in gravid women at high risk for birth defects. Am J Obstet Gynecol 2016; 152(7 Pt 1): 822-7.

13. Torres-Lagares D, Castellanos-Cosano L, Serrera-Figallo MÁ, García-García FJ, López-Santos C, Barranco A, Rodríguez-Gonzalez Elipe A, Rivera-Jiménez C, Gutiérrez-Pérez JL.. In Vitro and in Vivo Study of Poly(Lactic⁻co⁻Glycolic) (PLGA) Membranes Treated with Oxygen Plasma and Coated with Nanostructured Hydroxyapatite Ultrathin Films for Guided Bone Regeneration Processes. Polymers (Basel) 2017; 9(9): 410.

14. Zhang WJ, Zhang ZL, Chang JJ, Song XY. Prenatal ultrasonic diagnosis of absent pulmonary valve syndrome: A case report. Medicine (Baltimore) 2017; 96(35): e7747.

15. Leruez-Ville M, Ren S, Magny JF, Jacquemard F, Couderc S, Garcia P, Maillotte AM, Benard M, Pinquier D, Minodier P, Astruc D, Patural H, Ugolin M, Parat S, Guillois B, Garenne A, Parodi M, Bussières L, Stirnemann J, Sonigo P, Millischer AE, Ville Y. Accuracy of prenatal ultrasound screening to identify fetuses infected by cytomegalovirus which will develop severe long-term sequelae. Ultrasound Obstet Gynecol 2021; 57(1): 97-104.

16. Ambartsumyan L, Rodriguez L. Bowel management in children with spina bifida. J Pediatr Rehabil Med 2018; 11(4): 293-301.

17. Koerner J, Horvath D, Groettrup M. Harnessing Dendritic Cells for Poly (D,L-lactide-co-glycolide)

Microspheres (PLGA MS)-Mediated Anti-tumor Therapy. Front Immunol 2019; 10: 707.

18. Sami A, Naqvi SS, Qayyum M, Rao AR, Sabitaliyevich UY, Ahmad MS. Calcium based siRNA coating: a novel approach for knockdown of HER2 gene in MCF-7 cells using gold nanoparticles. Cellular and Molecular Biology 2020; 66(6): 105-11.
19. Alavi M, Adulrahman NA, Haleem AA, Al-Râwanduzi ADH, Khusro A, Abdelgawad MA, Ghoneim MM, Batiha GES, Kahrizi D, Martinez F, Koirala N. Nanoformulations of curcumin and quercetin with silver nanoparticles for inactivation of bacteria. Cell Mol Biol 2022; 67(5): 151-156.
20. Alavi M, Hamblin MR, Martinez F, Kennedy JF, Khan H. Synergistic combinations of metal, metal oxide, or metalloid nanoparticles plus antibiotics against resistant and non-resistant bacteria. Micro Nano Bio Aspects. 2022; 1(1): 1-9.
21. Song Y, Shi Y, Zhang L, Hu H, Zhang C, Yin M, Chu L, Yan X, Zhao M, Zhang X, Mu H, Sun K. Synthesis of CSK-DEX-PLGA Nanoparticles for the Oral Delivery of Exenatide to Improve Its Mucus Penetration and Intestinal Absorption. Mol Pharm 2019; 16(2): 518-532.
22. Sahu R, Dixit S, Verma R, Duncan SA, Coats MT, Giambartolomei GH, Singh SR, Dennis VA. A nanovaccine formulation of Chlamydia recombinant MOMP encapsulated in PLGA 85:15 nanoparticles augments CD4+ effector (CD44highCD62Llow) and memory (CD44highCD62Lhigh) T-cells in immunized mice. Nanomedicine 2020; 29: 102257.
23. Toledo MA, Wen TH, Binder DK, Ethell IM, Razak KA. Reversal of ultrasonic vocalization deficits in a mouse model of Fragile X Syndrome with minocycline treatment or genetic reduction of MMP-9. Behav Brain Res 2019; 372: 112068.